

# Preparation, and Evaluation of waste ground tyre rubber as Antioxidant, Antibacterial Activity and anticorrosion inhibitor for N80 steel in 0.1N H<sub>3</sub>PO<sub>4</sub>

Naeem T. Faili\*, Khawlah S. Burghal 

Department of Chemistry, College of Science, University of Basrah, Basrah, Iraq.

\*Corresponding Author.

Received 06/12/2022, Revised 02/06/2023, Accepted 04/06/2023, Published Online First 25/12/2023,  
Published 1/7/2024



© 2022 The Author(s). Published by College of Science for Women, University of Baghdad.

This is an open-access article distributed under the terms of the [Creative Commons Attribution 4.0 International License](https://creativecommons.org/licenses/by/4.0/), which permits unrestricted use, distribution, and reproduction in any medium, provided the original work is properly cited.

## Abstract

In this work, polybutadiene (PBD) was prepared from waste tires. The halogenated of polybutadiene was grafted with mono, di, and triethanolamine, the grafting was studied by X-ray diffraction and scanning electron microscopy. And according to the thermal characteristics (TGA and DSC), the produced compound was thermally stable up to 202 °C. Using potentiodynamic polarization techniques, the adsorption and corrosion inhibiting effects of three grafting polymers on N80 steel in 0.1 N H<sub>3</sub>PO<sub>4</sub> as aggressive environments were measured at four different temperatures: 25, 35, 45, and 55°C. The prepared polymers have excellent inhibition efficiency at high temperatures. The pBut-g-mono ethanol amine is the corrosion inhibitor that is most effective in all tested temperatures. The adsorption behavior of the polymers was found to follow the Langmuir isotherm, and the values of the free energy variation illustrate the mixed types of adsorptions occurring on the N80 surface. Tafel curves indicate that the tested polymers act as mixed anodic and cathodic inhibitors. In contrast, indicates that all tested modifying polymers had antioxidant capability.

**Keywords:** Diethanolamine, H<sub>3</sub>PO<sub>4</sub>, Monoethanolamine, N80 steel, Polarization instrument, Triethanolamine, waste tire.

## Introduction

A detrimental phenomenon, whether chemical or electrochemical, known as corrosion can attack any metal or alloy through reactivity with the environment, resulting in the loss of material properties or accelerated deterioration.<sup>1,2</sup>; in extreme situations, seriously harm infrastructure (pipelines, structures, bridges, and military bases), including cars and other mobile devices.<sup>3</sup>. Corrosion is caused by metals returning to their original states, such as iron converting to iron oxide in moist air.

Incorporating corrosion-protective (inhibiting) coatings and/or inhibitors is a crucial step in

corrosion control. Metal materials fail due to corrosion caused by the reaction of materials with their environment, which is a fundamental reason for global energy demand and sustainable development issues. Construction, shipping, manufacturing, and the chemical industries are all adversely affected by corrosion<sup>4</sup>. The use of inhibitors that are integrated into coatings or paints is one of the conventional techniques that are most frequently used. Inhibitors are substances that are applied as inhibiting compounds and utilized in low concentrations to prevent corrosion in industrial processes that involve contact with aqueous solutions<sup>5</sup>.

Polymers are used in anti-corrosion today, with organic chemicals being the most effective. Adsorption serves as the mechanism of inhibition, with the polar groups serving as the process' active centers<sup>6</sup>. Polymers have recently attracted a lot of interest as corrosion inhibitors due to their steadfast stability and expenditure. They form complexes when they interact with metal ions on the metal

## Materials and Methods

The chemicals were used without further purification and were obtained from trade exporters. Differential scanning calorimetric (DSC), thermal gravimetric analysis (TGA) and X-Ray diffraction were performed in department of chemistry, college science, University of Basra, Iraq. The antimicrobial examination was checked in the Biology Department, College of science, University of Basra, Iraq.

### Standard operating method for cutting GTR

After being cleaned with water to eliminate any dirt, the tires were set to air dry. Then, using a saw, the metal wires inside the tire's edges were removed and discarded. Afterward, the remaining parts of the tire were cut into small pieces using extremely sharp knives. The size of the tire chips was further reduced using an electric grinding machine.

### preparation for modifying GTR

A 4.0 g of ground tire rubber after treatment was added to 25 ml of bromine in carbon tetra chloride. The resulting mixture was stirred for 2 hours at low temperature (0°C). The brominated product was washed with ethanol and dried at 100 °C for 12 hours<sup>7, 8</sup>. To 6.0 g of brominated tire rubber, add 10 g of each mono, di, and triethanolamine, and then heat under reflux in an oil bath at 120 °C for 10 to 30 minutes. The resulting product was dried for 12 hours at 100 °C after being washed with distilled water<sup>8</sup>.

### Determination of Antioxidant Activity

The antioxidant activity of the synthesis polymer from GTR was evaluated using the  $\beta$ -carotene-linoleate model system. A mixture of 0.1 mg of  $\beta$ -carotene in 0.2 ml of chloroform, 10 mg of linoleic acid, and 100 mg of Tween-20 (polyoxyethylene sorbitan monopalmitate) were mixed. The chloroform was removed, and the resultant liquid was diluted with 10 mL of distilled water. Twenty milliliters of distilled water were added to this

surface via their functional groups. Polymers are used as metal corrosion inhibitors due to their extensive surface coverage and adsorption layer, protecting the metal from corrosive substances. The production of car tires is increasing due to the urgent need for them in the transport sector, leading to an increase in waste tires used in rubber production.

emulsion solution. 0.2 ml of extracts (50 and 100 ppm) and BHT (50 and 100  $\mu$ g) in ethanol were placed in separate test tubes, and 4 ml of the emulsion was pipetted into each test tube. For comparison, BHT was utilized. A control was created with 0.2 ml of ethanol and 4 mL of the above emulsion. The absorbance at 470 nm was measured at time zero (t=0) while the tubes were heated to 50 °C in a water bath. Until the color of  $\beta$ -carotene disappeared in the control tubes (t = 60 min), absorbance was measured every 15 minutes. As a control, a mixture devoid of  $\beta$ -carotene was prepared as described above. Every measurement was made three times. The extracts' antioxidant (AA) activity in terms of  $\beta$ -carotene bleaching was assessed using the following equation: Eq. 1, where  $A_0$  and  $A_t$  are the absorbance values measured at zero time of the incubation for the test sample and control, respectively. After incubation for 60 min,  $A_0$  and  $A_t$  are the absorbance measured in the test sample and control, respectively. The results were expressed on a percentage basis of preventing bleaching of  $\beta$ -carotene<sup>9</sup>

$$AA = 100[1 - (A_0 - A_t) / (A_0 - A_t)] \dots\dots\dots 1$$

### Antibacterial susceptibility of the synthesized polymers

Antibacterial activity was evaluated against two cultures of pathogenic bacteria (*Escherichia coli* and *Staphylococcus aureus*). At 37 °C for 24 hours, the bacterial culture was cultivated on nutritional agar. It was then administered, followed by another day of incubation. The diameter of the inhibitory zone was used to calculate the antibacterial activity<sup>10</sup>.

### Potentiodynamic polarization studies

The corrosion cell was composed of a flask with four nicks, two counter electrodes, a saturated calomel electrode (SCE), and a working electrode. To reduce IR drop, the working electrode's surface was made close to the tip of the Lugging capillary. An

appropriate holder was used to hold the circular disks with 1.1-1.2cm diameters and 3-4 mm thicknesses

were mechanically manufactured from N80 steel rod, which only had one side exposed to the electrolyte.

## Results and Discussion

### Characterization for Inhibitor

Diffraction is a physical phenomenon caused by the arrangement of atomic planes in a crystal lattice. The  $2\theta$  value and the corresponding interplanar spacing  $d$  are summarized. From the resulting XRD patterns, the broad diffraction peaks indicated that the structure performed a semi crystalline character  $d$  were determined from the position of the maximum  $2\theta$  of the broad peak. Bragg's equation ( $2d\sin\theta = n\lambda$ ) was used to calculate the average values of  $d$ . The properties of polymers depended mostly on the molecular weight, and crystallinity. XRD Commonly used to measure crystallinity, the crystallinity index CI can be calculated on the basis of an X-ray diffractogram. Postulating the following Eq.2 for determining the crystallinity index (CI):

$$CI\% = \frac{(I_m - I_{am})}{I_m} \times 100\% \dots\dots\dots 2$$

Where  $I_m$  (arbitrary units) is the maximum intensity of the crystalline peak at around  $2\theta$ , and  $I_{am}$  (arbitrary units) is the amorphous diffraction in most cases,  $CI$  provides information about the crystal state. crystallinity could also be assigned from an X-ray diffractogram by dividing the area of the crystalline peaks by the total area under curve<sup>11</sup>. The XRD of polybutadiene Fig.1 shows many peaks appear ( $2\theta = 31^\circ, 42^\circ, \text{ and } 50^\circ$ ). The crystallization rate is 60%. The characteristic diffraction peaks indicate the formation of modified GTR. The XRD technique can be used for the chemical analysis of modified polymer specimens using centroid peak, peak area and peak intensity as explained previously<sup>12</sup>, is little amorphous material as reported in the literature<sup>13</sup>.

(pBut-g-monoethanolamine) C1, many peaks appear ( $2\theta = 32^\circ, 38^\circ, 37^\circ, 39^\circ, 43^\circ, 59^\circ, 67^\circ, 62^\circ$  and  $66^\circ$ ).

(pBut-g-diethanolamine) C2 many peaks appear ( $2\theta = 38^\circ, 39^\circ, 43^\circ, 50^\circ, 49^\circ, 62^\circ, 53^\circ, 56^\circ, 62^\circ, 64^\circ$  and  $70^\circ$ ).

(pBut-g-triethanolamine) C3 many peaks appear ( $2\theta = 38^\circ, 39^\circ, 43^\circ, 50^\circ, 49^\circ, 62^\circ, 53^\circ, 56^\circ, 62^\circ, 56^\circ$  and  $66^\circ$ ).

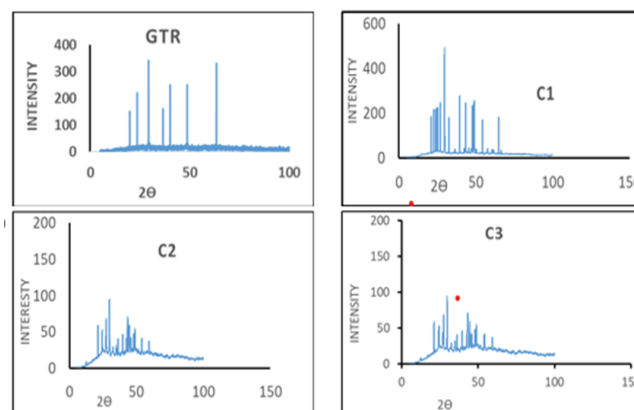


Figure 1. XRD patterns of GTR and C1, C2, & C3

### Thermogravimetric Analysis

One of the thermal analysis techniques used to investigate the thermal stability of a wide range of materials is thermal gravimetric analysis (TGA). Fig. 2 shows the GTR a weak peak at  $320^\circ\text{C}$  to 1%. The second peak is located at  $471^\circ\text{C}$  and is sharper and more prominent with a 13.76% residue of about 85%. In the thermogram, pBut-g-mono ethanol amine was observed to have three decomposition stages. The first one at  $278^\circ\text{C}$  Could be related to the degradation of 38%. The second one, at higher temperatures, with a peak around  $321^\circ\text{C}$ , can be related to the cleavage of the  $-\text{N}-\text{C}-\text{C}-$ band with weight loss of about 35%. The third peak is appreciated at  $490^\circ\text{C}$  with a mass loss of about 7.63%, which can be related to the degradation of the polymer, leaving the carbon residue of about 61%.

The pBut-g-diethanolamine (C2), three stages of decomposition, the first stage at  $271^\circ\text{C}$  is related to the loss of water molecules (3.75%). The second stage at  $374^\circ\text{C}$  can be related to the loss of the 5% wt cleavage of the methylene group. The third stage is equivalent to 5.63% wt. loss at  $472^\circ\text{C}$  and corresponds to the depolymerization of diethanolamine and polybutadiene rubber with a remaining 86.78% wt. of carbon. In the thermogram, three decomposition stages of pBut-g-triethanolamine (C3) were observed. The first, equivalent to 9% wt. % loss at  $67^\circ\text{C}$ , could be due to the loss of a volatile component present. The second one is at higher temperatures, with a peak around  $175^\circ\text{C}$ .

°C to the cleavage of the —N-C-C-band with a weight loss of about 2%. The third peak is appreciated at 463 °C with a mass loss of about 17.63%, which can be related to the degradation of

chains, leaving a carbon residue of about 51.4%. While the modified polymers from ground tier rubber pBut > C3 > C2 > C1 more stable.

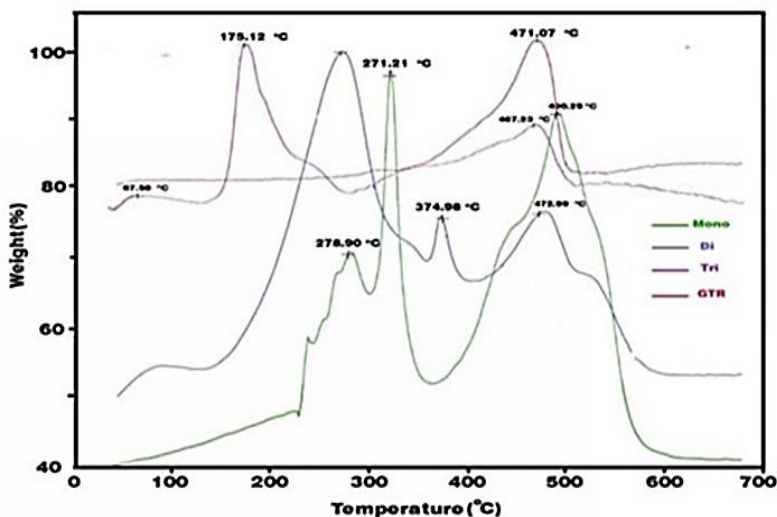


Figure 2. TGA for GRT and C1, C2 & C3

### Differential Scanning Calorimetry (DSC)

The DSC data for modifying GTR in Table 1 show two endothermic peaks, a broad peak centered at about 74 C and the loss of water associated with the hydrophilic groups of the polymer. The second endothermic peak, 207 C°, corresponded to the chemical bond decomposition of polybutadiene rubber. The DSC thermogram of C1 exhibited a broad endothermic peak centered at about 145 C. The exothermic peak, which appears in the temperature range between about 172 C and 172 C, corresponds to the decomposition of the polymer C1. The DSC

thermogram of C2 is shown, which shows a broad endothermic peak at 66 C, which corresponds to the removal of ammonia. The glass transition temperature appears in a small endothermic peak at about 195 C°. The endothermic peak that appears in the temperature range of about 323 C° corresponds to the decomposition of the polymer C2. The C3 DSC thermogram showed an exothermic peak of 151 C°, corresponding to the loss of ammonia at about 216 C, and the glass transition temperature appears to be a medium exothermic peak at about 216 C°.

Table 1. The DSC parameters for Modifying polymer

polymer	Phase transition of decomposition temperature											
	Ti	Top	Tf	ΔH J/g	Ti	Top	Tf	ΔH J/g	Ti	Top	Tf	ΔH J/g
pBut	36	74	102	-11.88	207	207	207	-18.81	36	74	102	-11.88
C1	119	145	172	-55.7	-	-	-	-	-	-	-	-
C2	31	66	110	-647	179	195	287	-176	314	327	337	-17
C3	141	150	167	-186	171	216	216	-207.2	-	-	-	-

### The Antioxidant Activity β-Carotene Assay

The antioxidant properties of the examined compounds are evaluated from kinetics curves (absorbance vs. time Fig. 3) for the modified polymer and the control. In this method, antioxidant activity is most frequently expressed as a percentage inhibition relative to the control, which is free of the examined antioxidant as shown in Table 2. This graph depicts the β-carotene assay rates of the

control and modifying polymers. It shows a decrease in the absorbance of β-carotene in the presence of different modifying polymers due to the oxidation of β-carotene and linoleic acid. The three polymers showed a decrease in the adsorbed of β-carotene due to the oxidation of β-carotene and linoleic acid.

This shows that rapid industry growth has not only increased production but also led to the release of hazardous compounds into the environment, posing

health risks. It has significantly impacted how the environment functions normally<sup>14, 15</sup>. Synthetic polymers from GTR with biomolecules have gained attention in recent technologies due to their biodegradability, biocompatibility, low toxicity, and affordability. The applications for these characteristics range from plastic bags and packaging to biomedical disciplines like bone plates, fixation screws, or sutures.<sup>14, 16</sup>

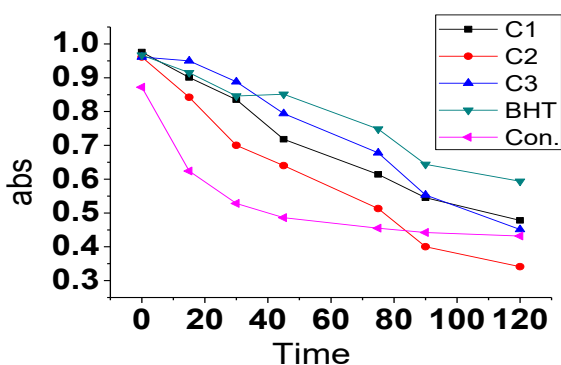


Figure 3. Possessed antioxidant capacity

Table 2. Antioxidant results

Comp.	A <sub>j</sub>	A <sub>t105</sub>	A <sub>j</sub> *	A <sub>t</sub> *	% AA
BHT	1.728	1.528	0.872	0.432	95.20
C1	0.976	0.21	0.872	0.432	70
C2	0.973	0.161	0.872	0.432	78
C3	0.970	0.151	0.872	0.432	80

### Antibacterial Susceptibility of the modifying polymer

Infections are mostly caused by microbes, which include live organisms like bacteria and fungi. Pathogenic bacteria cause infectious diseases, which are the leading cause of death worldwide<sup>17</sup>. The antibacterial activity of all the modified polymers from ground tire rubber was performed against two bacterial strains. The positive, *Staphylococcus aureus*, and the negative, *Escherichia coli*, Zones of inhibition were measured. All dilutions were made in dimethyl sulfoxide (DMSO). This solvent has no inhibitory effects on the growth of bacteria. Antibacterial activity was evaluated based on the absence or presence of bacterial growth in the area between the agar and the specimens (the inhibition

zone), as well as the shape and size of the inhibition zone that formed around the specimens, and on the evaluation of bacterial growth under the sample<sup>18</sup>. Membranolytic characteristics, rather than simply changing the surface tension of the extracellular media, are the mode of action of antibacterial actions, which is affected by microbial density<sup>19, 20</sup>. The occurrence and rise of antibiotic resistance in microbial. Resistance can come from within, be acquired by spontaneous mutations (de novo), or come from donor bacteria, phages, or free radicals. The inhibition of the antibiotic's initial penetration of the bacterial cell wall or expulsion before the antibiotic reaches its target by certain flux pumps are actions related to intrinsic or innate resistance<sup>21</sup>.

### Effect of concentration

Fig. 4 shows the cathodic and anodic polarization curves of N80 steel at 298 K and 0.1N H<sub>3</sub>PO<sub>4</sub> for C1, C2 and C3 in the presence and absence of inhibitory polymers at various concentrations. Both cathodic and anodic currents are seen to be decreasing as increasing the inhibitor polymer concentration results in a decrease in I<sub>corr</sub> values relative to those in the uninhibited solution. This result implies that the dissolving of steel and hydrogen ions is regulated by the addition of polymers at the same time<sup>22</sup>.

Additionally, Table 3 illustrates how the corrosion rate values of N80 steel in 0.1N H<sub>3</sub>PO<sub>4</sub> decrease as the concentration of polymers increases<sup>23, 24</sup>. The inhibitor adsorption process depends on several factors like the plane of the compound, the planarity of the compound, lone pairs present in hetero atoms, multiple bonds, steric hindrance, etc. A protective layer is quickly formed on the metal surface through the metal/solution interface when polymers are added. From Table 3, it is also clear that the order of increasing inhibition efficiency is C1 > C2 > C3. The crowding surrounding the N-atom grows as the number of ethanol groups and polymer chains on the N-atom rises. The strain caused by this crowding is the least in C1 and greatest in C3. Because of this, C1 has higher molecular stability than C3, which also reduces basicity. Due to this action, C1 provides greater inhibition in this acid than C2 and C3<sup>25</sup>.

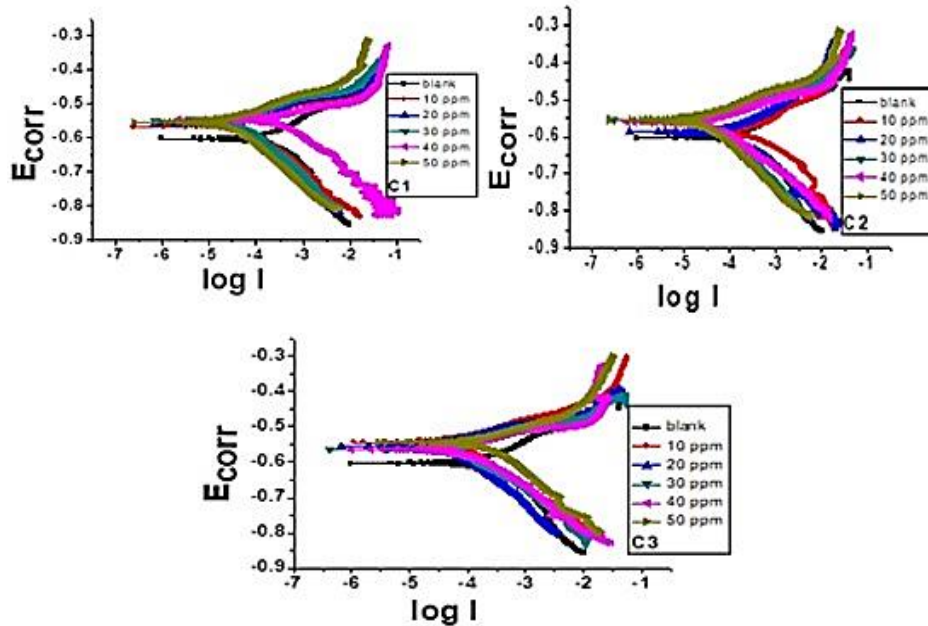


**Figure 4. Potentiodynamic polarization curves for corrosion of 80 steel in 0.1N H<sub>3</sub>PO<sub>4</sub> in the absence and presence of different concentrations from C1, C2& C3 at 298**

**Table 3. Electrochemical data from the Tafel plot method, in absence and presence of inhibitors, at different concentrations and 298K.**

Comp.	Conc. ppm	-E <sub>corr</sub> mV	-β <sub>c</sub> mV. decade <sup>-1</sup>	β <sub>a</sub> mV decade <sup>-1</sup>	R <sub>p</sub> Ω.CM <sup>2</sup>	I <sub>corr</sub> μA.CM <sup>-2</sup>	CR mpy	Eff.%
blank	3266	0.60304	78.736	130.38	86.717	228.57	139.30	
C1	10	0.56745	55.762	75.224	243.82	64.14	29.37	78.91
	20	0.55894	47.941	101.4	237.21	55.03	25.48	81.70
	30	0.54924	48.319	110.51	331.29	39.49	18.25	86.89
	40	0.55272	51.601	74.044	355.04	33.80	15.65	88.76
	50	0.55454	52.374	113.31	390.37	27.20	12.59	90.95
C2	10	0.58591	69.593	76.411	214.07	72.13	33.03	76.28
	20	0.58878	76.695	103.35	279.6	61.30	28.07	79.84
	30	0.55414	48.923	107.12	312.26	28.54	25.88	81.42
	40	0.56188	49.883	90.329	332.91	41.31	18.92	86.41
	50	0.55908	46.997	95.029	366.67	40.74	18.65	86.61
C3	10	0.54426	54.021	112.8	206.28	99.79	35.26	74.68
	20	0.55687	48.226	109.53	332.91	74.59	34.54	75.20
	30	0.56405	51.902	96.649	341.68	66.95	31.00	77.74
	40	0.56291	43.232	84.01	362.04	51.96	24.06	82.72
	50	0.56160	38.48	70.745	374.35	42.98	20.09	85.57

### Effect of temperature

To investigate the variation of temperature on the corrosion of N80 steel, Potentiodynamic polarization measurements were performed in the temperature range of 298–328 K in the absence and presence of polymeric inhibitors. The data in Table 4 shows that the corrosion rate for both inhibitors and uninhibitors increases as the solution's temperature rises. This leads to a reduction in the evaluated inhibitory

polymers' ability to prevent corrosion. The evaluated inhibitors exhibited inadequate protection at the highest temperatures. This result implies that the temperature increase prevented physical interactions (physisorption), which decreased the protective efficiency<sup>26</sup>. Adsorption of inhibitors can slow the rate of corrosion by minimizing the area that can be used for reactions (geometric blocking effect) or by altering the activation energy. During the inhibited

corrosion process of the anodic and/or cathodic processes occurring on the inhibitor-free surface, the following equations were used to derive the activation parameters for the corrosion process using an Arrhenius type plot<sup>27, 28</sup> in Eqs. 3,4.

$$\ln CR = \log A - \left(\frac{E_a}{R}\right) \dots\dots\dots 3$$

$$\ln C.R = \left(\frac{\Delta S}{R}\right) + \frac{\Delta H}{RT} + \ln\left(\frac{R}{Nh}\right) \dots\dots\dots 4$$

CR is the corrosion rate,  $E_a$  is the apparent activation energy for the corrosion process, R is the molar gas constant, T is the absolute temperature, and A is the pre-exponential factor. The Planck's constant is h, the Avogadro number is N, and the enthalpy and entropy changes of the activation corrosion energies for the transition are H and Sa, respectively.

When plotting (ln C.R) vs. (1/T) Fig. 5 for the inhibitory polymers, straight lines were produced with the intercept of A and sloping (-EA/R), from which  $E_a$  calculated and listed in Table 5. The results presented show that the value of  $E_a$  for inhibited solutions is higher than that obtained for blank solutions. chemical adsorption that occurs in the first stage could be the cause of the increase in apparent activation energy<sup>29</sup>. It was discovered that the variance of apparent activation energy and the pre-exponential factor (A) are comparable.

In previous investigations, similar results have been seen<sup>30, 31</sup>. Researchers<sup>32</sup> found that the increase in activation energy can be attributed to a perceptible decrease in the adsorption of the inhibitor on the N80 steel surface with an increase in temperature. Because these two reverse processes are in

equilibrium, more inhibitor molecules desorb as adsorption decreases. An important N80 steel surface comes into contact with a hostile environment because more inhibitor molecules are desorbing at higher temperatures, which cause increased corrosion rates as temperature rises<sup>33, 34</sup>. Plotting (ln C.R/T) vs. (1/T) gave a straight line with intercepts ( $\ln(R/Nh) + \Delta S/R$ ) and slopes of (- $\Delta H/R$ ) that were used to derive the values of  $\Delta S$ , and  $\Delta H$  as shown in Table 5 Fig.5 The endothermic nature of the metal dissolving process is reflected by the positive values of  $\Delta H$  in the absence and presence of the inhibitor, suggesting that mild steel dissolves slowly<sup>35, 36</sup>. The table clearly indicates that the value of  $\Delta H$  increased when inhibitors were added compared to the uninhibited solution, indicating a higher degree of protection. In accordance with the negative values of activation entropy in the absence and presence of inhibitors<sup>37,38</sup>, the formation of the activated complex in the rate-determining step represents an association rather than a dissociation step. This assumes that disorder decreases during the transition from reactants to activated complexes<sup>39</sup>.

**Table 4. Polarization parameters and the corresponding inhibition efficiency for N80 steel in 0.1 N H<sub>3</sub>PO<sub>4</sub> in the absence and presence of optimum concentration at different temperatures.**

Comp.	Temp	-E <sub>corr</sub> mV	$\beta_a$ mV .decade <sup>-1</sup>	$-\beta_c$ mV .decade <sup>-1</sup>	R <sub>p</sub> Ω.CM <sup>2</sup>	I <sub>corr</sub> μA.CM <sup>-2</sup>	CR mpy	Effe. %
blank	298	0.60304	78.736	130.38	86.717	303.83	139.30	
C1		0.55454	52.374	113.31	390.37	27.202	12.59	90.95
C2		0.55908	46.997	95.029	366.67	40.737	18.65	86.61
C3		0.56160	38.48	70.745	374.35	42.978	20.09	85.57
blank	308	0.59475	98.865	123.32	60.404	598.23	274.01	
C1		0.57044	49.764	95.726	208.65	75.353	34.89	87.26
C2		0.56462	42.636	85.247	217.61	101.17	46.33	83.08
C3		0.55462	35.511	77.843	235.47	110.78	51.26	81.29
blank	318	0.55064	98.716	198.8	38.119	833.38	385.92	
C1		0.55229	61.852	115.28	118.03	137.19	63.53	83.63
C2		0.55441	54.398	207.44	158.9	164.18	76.02	80.29
C3		0.54129	69.747	141.89	115.39	180.78	82.80	78.54
blank	328	0.57325	73.498	92.428	24.44	1067.4	494.29	
C1		0.54891	67.509	125.13	91.577	198.31	91.83	81.42
C2		0.57089	62.844	79.709	40.002	230.74	104.71	78.81
C3		0.54471	81.398	170.21	71.289	257.49	116.62	76.40

**Table 5. Thermodynamic Parameters of mild steel corrosion in 0.1N H<sub>3</sub>PO<sub>4</sub>**

sample	ΔS J.mol.K <sup>-1</sup>	ΔH KJ.mol <sup>-1</sup>	ΔE KJ/mol	K <sub>ads</sub> (M <sup>-1</sup> )	ΔG KJ/mol
C1	-53.58	50.52	47.526	50000	-36.757
C2	-73.98	43.14	46.308	50000	-36.757
C3	-71.20	43.79	53.032	33333.33	-35.753
un	-99.15	31	43.15		

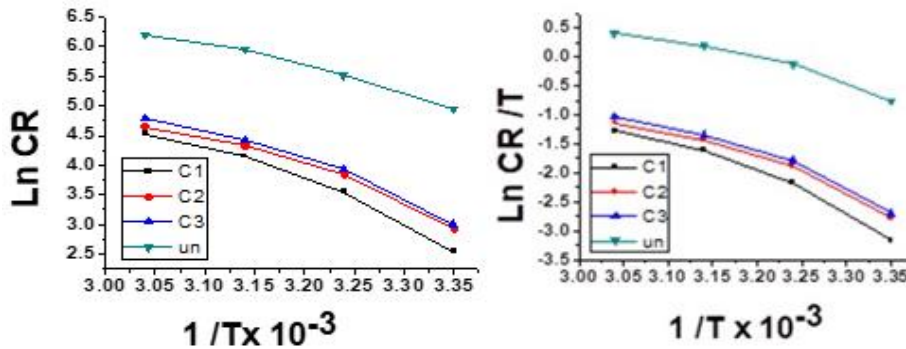


**Figure 5. Transition Arrhenius plots of N80 steel in 0.1 N H<sub>3</sub>PO<sub>4</sub> with and without inhibitory polymers**

**Adsorption isotherm:**

The adsorption of inhibitory polymers was studied on the surface of the alloy, and the obtained results showed that the adsorption follows the Langmuir isothermal model. Due to the fact that adsorption is a surface phenomenon, an adsorption isotherm was utilized to study the adsorption process. The difference in the amount of inhibitor that the adsorbent absorbed with concentration at constant temperature is represented by the adsorption isotherm in the graph as shown in Eq .5

$$\frac{C_{inh}}{\theta} = \frac{1}{K_{ads}} + C_{inh} \dots\dots\dots 5$$

Where C<sub>inh</sub> is the concentration of the inhibitor, θ is the degree of surface coverage, and K<sub>ads</sub> is the adsorption equilibrium constant. linear relationships Fig. 6 depicts the transition from C<sub>inh</sub>/θ to C<sub>inh</sub>. Strong polymer adsorption on the metal surface, which results in the formation of a shielding layer that separates the alloy's surface from the surrounding acidic media, is indicated by a high value for K<sub>ads</sub><sup>40</sup>. The standard free energy of adsorption ΔG<sub>ads</sub> is computed using the equilibrium constant of adsorption K<sub>ads</sub>, according to Eq. 6.<sup>41</sup>

$$\Delta G_{ads} = RT \ln (55.5 K_{ads}) \dots\dots\dots 6$$

**Conclusion**

Grafting polymers have been manufactured and applied as a successful corrosion inhibitor for N80 steel in 0.1 phosphoric acid media. The synthesis of

The negative ΔG<sub>ads</sub> values show strong interactions between inhibitor molecules and the metal surface<sup>42</sup>, in addition to spontaneous polymer adsorption onto the N80 steel surface<sup>43</sup>. This study's ΔG<sub>ads</sub> results for C1, C2, and C3 were all slightly over -20 kJ mol<sup>-1</sup> but below -40 kJ mol<sup>-1</sup>, indicating a mixed-type binding process on the N80 surface with a predominating chemisorption mechanism as the values go closer to the -40 kJ mol<sup>-1</sup> value. This indicates that the physical to chemical type adsorption mechanism has received some alteration ΔG<sub>ads</sub> (-) results are in favor of the spontaneous kind of binding process<sup>44</sup>.

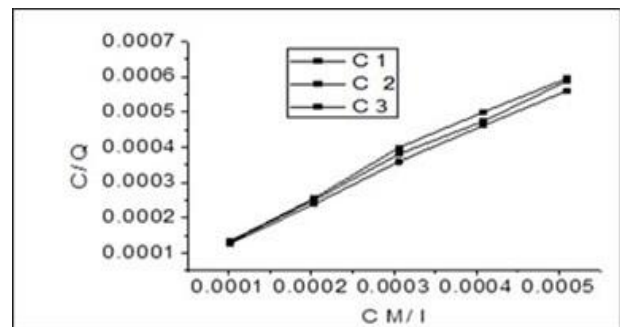


**Figure 6. Langmuir isotherm adsorption model of C1, C2 and C3 on the surface of N80 steel in 0.1 N H<sub>3</sub>PO<sub>4</sub>.**

branched polymers was verified by the results of TGA, DSC, and powder XRD examinations. Electrochemical experiments and studies showed

that synthesized polymers have excellent acidic corrosion-inhibiting characteristics for N80 steel. The best inhibitor, C1, has an inhibition efficiency of 90%, followed by C2, and C3. The inhibited solution's corrosion activation energy was higher than that of the uninhibited solution. The entropy of activation reflects a decrease in the rate of metal dissolution, whereas the positive sign of enthalpy of activation reflects endothermic metal dissolution. The branched polymers that were created follow the

### Acknowledgment

The authors are grateful to the Department of Chemistry, College of Science/University of Basrah for providing the chemicals and corrosion measuring

### Authors' Declaration

- Conflicts of Interest: None.
- We hereby confirm that all the Figures and Tables in the manuscript are ours. Furthermore, any Figures and images, that are not ours, have been included with the necessary permission for republication, which is attached to the manuscript.

### Authors' Contribution Statement

K.S. contribution involved the preparation of polymers as well as the investigation and writing of their effects as antioxidants and anti-bacterial, whilst

Langmuir adsorption isotherm. Measurements of potentiodynamic polarization revealed that all the polymers work as mixed-type inhibitors, inhibiting both cathodic and anodic processes simultaneously. The three modified polymers showed high inhibitory efficacy against pathogenic bacteria within the minimum inhibitor concentration, As a result of  $\beta$ -carotene and linoleic acid oxidation, they exhibited a decrease in the amount of  $\beta$ -carotene adsorbed.

tools as well as Prof. Dr. Salah Shaker for his support throughout the research

- Authors sign on ethical consideration's approval.
- Ethical Clearance: The project was approved by the local ethical committee at University of Basrah.

### References

1. Raker EJ. National hazards, disasters, and demographic change: The case of Severe tornadoes in the United States, 1980-2010. *Demogr.* 2020; 57(2): 653-674. <https://doi.org/10.1007/s13524-020-00862-y>
2. Zheng YE, Xie Y, X Long, A comprehensive review of Bayesian statistics in natural hazards engineering. *Natural Hazards.* 2021; 108(1): 63-91. <https://doi.org/10.1007/s11069-021-04729-22>
3. Rodrigues R, Gaboreau S, Gance J, Lgnatiadis I, Betelu,S. Reinforced concrete structures: A review of corrosion mechanisms and advances in electrical methods for . corrosion monitoring. *Constr Build Mater.* 2021; 269: 121240. <https://doi.org/10.1016/j.conbuildmat.2020.121240>.
4. Liu H, Cao F, Song G-Ling, Zheng D, Shi Z, Dargusch MS, et al. Review of the Atmospheric corrosion of magnesium alloys. *J. Mater. Technol.* 2019; 35(9): 2003-2026. <https://doi.org/10.1016/j.jmst.2019.05.001>
5. Ali AM, Thair L, Intisar J. Studying Biomimetic Coated Niobium as an Alternative Dental Implant Material to Titanium (in vitro and in vivo study). *Baghdad Sci J.* 2018; 15(3): 253-261. <https://doi.org/10.21123/bsj.2018.15.3.0253>
6. Idumah, C.I, Obele CM, Emmanuel EO, Hassan A. Recently emerging nanotechnological advancements in polymer nanocomposite coatings for anti- corrosion, anti-fouling and self healing. *Surf Interfaces.* 2020; 21: 100734. <https://doi.org/10.1016/j.surfin.2020.100734>
7. Murry DJ, Gorman DB, Jr JWH, Jr JWK, Morgan TA, King BA, et al. Process for brominating butadiene/vinyl aromatic copolymer. U S. Patent: 2012; US00811493B2.
8. Kocevski S, Yagneswaran S, Xiao F, Punith VS, Jr DWS, Amirkhanian S. Surface modified ground rubber tire by grafting acrylic acid for paving applications, *Constr Build Mater.* 2012; 34: 83-9 <https://doi.org/10.1016/j.conbuildmat.2012.02.040>

9. Ibrahim EA, Omran AA, Salama Za. Evaluation of Turkish Delight Prepared with Pigments and Essential Oils Extracted from Clementine (Citrus Clementine) Peels as Natural Antioxidants, *Baghdad Sci J*. 2022; 19(4): 745-752, <https://doi.org/10.21123/bsj.2022.19.4.0745>
10. Poirrel L, Jayol A, Nordmann P. Polymyxins: antibacterial activity, susceptibility testing, and resistance mechanisms encoded by plasmids or chromosomes, *Clin Microbiol Rev*. 2017; 30: 557-596. <https://doi.org/10.1128/CMR.00064-16>.
11. Sari N H, Wardana ING, Irawan YS, Siswanto E. Characterization of the chemical, physical, and mechanical properties of NaOH-treated natural cellulosic fibers from corn husks. *J Nat Fibers*. 2018; 15(4): 545-558. <https://doi.org/10.1080/15440478.2017.1349707>
12. Khordehbinan M, Kaymanesh MR, Chemical analysis and middle-low temperatur functional of waste polybutadiene rubber polymer modified bitumen. *Pet Sci Technol*.2020; 38(1): 8-17. <https://doi.org/10.1080/10916466.2019.1608237>
13. Maiti M, Basak GC, Srivastava VK, Jasra RV. Mesoporous silica reinforced polybutadiene rubber hybrid composite. *Int J Ind Chem*.2016; 7(2): 131-141. <https://doi.org/10.1007/s40090-015-0062-8>
14. Jia X, Ge Y, Shao L, Wang C, Wallac GG. Tunable conducting polymers: toward sustainable and versatile batteries. *ACS Sustain Chemi Eng*. 2019; 7(17): 14321-14340. <https://doi.org/10.1021/acssuschemeng.9b02315>
15. Raj M. Natural antioxidant (flavone glycoside) from Emilia sonchifolia DC. And its potential activity. *Int J Pharm Sci*. 2012; 4(1): 159-162. <https://innovareacademics.in/journal/ijpps/Vol4Supp13/3576.pdf>
16. Jahangirian H, Azizi S, Moghaddam RR, Baratavand B, Webster TJ. Status of plant protein-based green scaffolds for regenerative medicine applications. *Biomolecules*. 2019; 9(10): 619. <https://doi.org/10.3390/biom9100619>
17. Chourifa H, Bouloussa H, Migonney V, Daudre CF. Review of titanium surface modification techniques an coatingsfor antibacterial applications. *Acta biomater*. 2019; 83: 37-54. <https://doi.org/10.1016/j.actbio.2018.10.036>
18. Bereksi MS, Hassain H, Bekhechi C, Abdelouahid DE. Evaluation of antibacterial activity of some medicinal plants extracts commonly used in Algerian traditional medicine against some pathogenic bacteria. *Pharmacogn J*. 2018; 10(3): 507-512. <https://doi.org/10.5530/pj.2018.3.83>
19. Roger T, Marie M P, Igor V K, Patric V D. Phytochemical screening and antibacterial activity of medicinal plants used to treat typhoid fever in Bamboutos division, West Cameroon. *J Appl Pharm Sci*. 2015; 5(6): 034-049. <https://doi.org/10.7324/JAPS.2015.50606>
20. Shendurse AM, Sangwan RB, Amit K, Ramesh V, Patel AC, Gopikrishna G, et al. Phytochemical screening and antibacterial activity of lemongrass (Cymbopogon citratus) leaves essential oil. *J Pharmacogn Phyto*. 2021; 10(2): 445-449.
21. Salayová A, Bedlovicva Z, Daneu N, Balaz M, Bujnakova ZL, Balasova L, et al. Green synthesis of silver nanoparticles with antibacterial activity using various medicinal plant extracts: Morphology and antibacterial efficacy. *Nanomaterials*. 2021; 11(4): 1005. <https://doi.org/10.3390/nano11041005>
22. ChaouiKi A, Chafiq M, Lgaz H, Bhat S, Ali IH, Manoor S, et al. Experimental and theoretical insights into the corrosion inhibition potential activity of a novel pyrazoline derivatives for mild steel in 1M. HCl. *Appl J Envir Eng Sci*. 2020; 6(1):79-93, <https://doi.org/10.48422/IMIST.PRSM/ajees-v6i1.20261>
23. Abd El-Lateef HM, Shalabi K, Arab AM, bdallah YM. Corrosion Mitigation Performance of N80 Steel in 5% Sulfamic Acid Medium byApplying Novel Tetrahydro-1,2,4-triazines Including Triazene Moieties: Electrochemical and Theoretical Approaches. *ACS Omega*. 2022; 7: 23380–23392. <https://doi.org/10.1021/acsomega.2c01629>
24. Zhang W, Li HJ, Wang Y, Liu Y, Wu YC. Adsorption and corrosion inhibition properties of pyridine-2-aldehyde-2- quinolylhydrazone for Q235 steel in acid medium: Electrochemical, thermodynamic, and surface studies. *Mater Corros*. 2018; 69: 1638–1648. <https://doi.org/10.1002/maco.201810252>
25. Vashi RT, Bhajiwala HM, Desai SA. Ethanolamines as corrosion inhibitors for Zinc in (HNO<sub>3</sub>+ H<sub>2</sub>SO<sub>4</sub>) binary acid mixture. *J Chem*. 2010; 7(2): 665-668. <https://doi.org/10.1155/2010/518543>
26. Dohare P, Quraishi MA, Verma C, Lgaz H, Salghi R, Ebenso E. Ultrasound induced green synthesis of pyrazolo-pyridines as novel corrosion inhibitors useful for industrial pickling process: Experimental and theoretical approach. *Results Phys*. 2019; 13: 102344. <https://doi.org/10.1016/j.rinp.2019.102344>
27. Mazkour A, Hajjaji EI, Labjar N, Lotfi EI, Mahi M. Investigation of Corrosion Protection of Austenitic Stainless Steel in 5.5M Polluted Phosphoric Acid Using 5- Azidomethyl-7-morpholinomethyl-8-hydroxyquinoline as an Ecofriendly Inhibitor. *Int J Corros*. 2021: 6666811- 6666825. <https://doi.org/10.1155/2021/6666811>
28. Chadili M, Rguiti MM, El Ibrahim B, Oukhtib R, Jmiai A, Beelkhaouda M, et al., Corrosion Inhibition of 3003 Aluminum Alloy in Molar Hydrochloric Acid Solution by Olive Oil Mill Liquid By-Product. *Int J Corros*. 2021: 6662395–6662407. <https://doi.org/10.1155/2021/6662395>
29. Zeena Sh. Abeer K.Taghried A. Study the Inhibition Effect of Amoxicillin Drug for Corrosion of Carbon Steel in Saline Media. *Baghdad Sci J*. 2022; 19 (1):

- 121-131.  
<https://doi.org/10.21123/bsj.2022.19.1.0121>
30. Chaouiki A, Chafiq M, Ko YG, Thari FZ, Salghi R, Karrouchi K, et al. Adsorption Mechanism of Eco-Friendly Corrosion Inhibitors for Exceptional Corrosion Protection of Carbon Steel: Electrochemical and First-Principles DFT Evaluations. *Metals*. 2022; 12(10): 1598. <https://doi.org/10.3390/met12101598>
31. Hegazy M, Ahmed HM, El-Tabei AS. Investigation of the inhibitive effect of p-substituted 4- (N, N, N-dimethyldodecylammonium bromide) benzylidene-benzene-2-yl-amine on corrosion of carbon steel pipelines in acidic medium. *Corros Sci*. 2011; 53(2): 671-678. <https://doi.org/10.1016/j.corsci.2010.10.004>
32. Mahdi BS, Abbass MK, Mohsin MK, Al-Azzawi WK, Hanoon MM, Al-Kaabi MHH, et al. Corrosion inhibition of Mild Steel in Hydrochloric Acid Environment Using Terephthaldehyde Based on Schiff Base Gravimetric, Thermodynamic, and Computational Studies. *Molecules*. 2022; 27(15): 4857. <https://doi.org/10.3390/molecules27154857>
33. Verma C, Sorour AA, Ebenso EE, Quraishi MA. Inhibition performance of three naphthyridine derivatives for mild steel corrosion in 1 M HCl: Computation and experimental analyses. *Results Phys*. 2018; 10: 504-511. <https://doi.org/10.1016/j.rinp.2018.06.054>
34. Mishra A, Verma C, Lgaz H, Srivastava V, Quraishi M, Ebenso Synthesis, characterization and corrosion inhibition studies of N-phenyl- benzamides on the acidic corrosion of mild steel: Experimental and computational studies. *J Mol Liq*. 2018; 251: 317-332. <https://doi.org/10.1016/j.molliq.2017.12.011>
35. Tavakoli P, Shadizadeh SR, Hayati F, Fattahi M. Effects of synthesized nanoparticles and Henna-Tragacanth solutions on oil/water interfacial tension: nanofluids stability considerations. *Pet*. 2020; 6(3): 293-303. <https://doi.org/10.1016/j.petlm.2020.03.001>
36. Li D, Zhang P, Guo X, Zhao X, Xu Y. The inhibition of mild steel corrosion in 0.5 M H<sub>2</sub>SO<sub>4</sub> solution by radish leaf extract. *Rsc Adv*. 2019; 9: 40997. <https://doi.org/10.1039/C9RA04218K>
37. Priya M, Senthil M. Study of Inhibitive Action of Biodegradable Crab Shell Extract on Mild Steel in Acidic Medium. *Egypt J Chem*. 2022; 65(5): 93-100. <https://doi.org/10.21608/EJCHEM.2021.88826.4277>
38. Chen Y, Chen Z, Zhuo Y. Newly Synthesized Morpholinyl Mannich Bases as Corrosion Inhibitors for N80 Steel in Acid Environment. *Materials* 2022; 15: 4218. <https://doi.org/10.3390/ma15124218>.
39. Kubba RM, Mohammed MA, Ahamed LS. DFT Calculations and Experimental Study to Inhibit Carbon Steel Corrosion in Saline Solution by Quinoline-2-One Derivative. *Baghdad Sci J*. 2020; 18(1): 113-123. <https://doi.org/10.21123/bsj.2021.18.1.0113>.
40. Lively RP, Sholl DS. From water to organics in membrane separations. *Nat Mater*. 2017; 16(3): 276-279. <https://doi.org/10.1038/nmat4860>
41. Hay MA, Balakit AA, Salman HI, Abdulridha AA, Sert Y. New heterocyclic compound as carbon steel corrosion inhibitor in 1M H<sub>2</sub>SO<sub>4</sub>, high efficiency at low concentration: Experimental and theoretical studies. *J Adhes Sci Technol*. 2022; 37(40): 1-23. <https://doi.org/10.1080/01694243.2022.2034588>
42. Talat R, Asghar MA, Tariq I, Akhter Z, Liaqat F, Nadeem L, et al. Evaluating the Corrosion Inhibition Efficiency of Pyridinium-Based Cationic Surfactants for EN3B Mild Steel in Acidic-Chloride, Media. *Coatings*. 2022; 12: 1701. <https://doi.org/10.3390/coatings12111701>.
43. Yang D, Feng X, Yan N, Wang Y, Lu L, Mei P, et al. Corrosion Inhibition Studies of Benzoxazole Derivates for N80 Steel in 1 M HCl Solution: Synthesis, Experimental and DTF Studies. *OJO Gas*. 2022; 7: 101-123. <https://doi.org/10.4236/ojogas.2022.72007>
44. Yousef TA, Hussein RH, Alhamzani AG, Al-Enazi AT, Al-Osimi MB, Abou-Krishna MM. Environment-friendly Corrosion Inhibitors for Aluminum in Hydrochloric Acid: Quantum and experimental Research. *Metals*. 2022; 12:1538. <https://doi.org/10.3390/met12091538>

## تحضير وتقييم بوليمرات رخيصة كمضادات للبكتريا، الاكسدة ومثبطات تاكل لسبيكة من نوع N80 في تركيز 0.1N من حامض الفسفوريك

نعيم تقي فيلي، خولة صبيح برغال

قسم الكيمياء، كلية العلوم، جامعة البصرة، البصرة، العراق.

### الخلاصة

في هذا العمل، تم تحضير بولي بوتادين (PBD) من نفايات الاطارات. وطعم البولي بوتادين المهلجن باستخدام أحادي وثنائي وثلاثي إيثانول امين، ودرس التطعيم عن طريق حيود الأشعة السينية والمسح المجهر الإلكتروني. وتشير الخواص الحرارية (TGA, DSC) إلى أن المركبات المحضرة تمتلك ثباتاً حرارياً حتى 202 درجة مئوية. باستخدام تقنيات الاستقطاب الديناميكي الفعال، تم قياس تأثيرات الامتزاز والتآكل للبوليمرات الثلاثة المطعمة على فولاذ N80 في  $H_3PO_4$  0.1N في اربع درجات حرارية مختلفة : 25 و 35 و 45 و 55 درجة مئوية. وقد اظهرت البوليمرات المحضرة كفاءة تثبيط ممتازة عند درجات الحرارة المختلفة. يعتبر pBut-g-mono ethanol amine هو الأكثر فعالية كمثبط للتآكل في جميع درجات الحرارة المختبرة. كما ان سلوك الامتزاز للبوليمرات الثلاث تخضع لمخطط لانجموير، وقيم الطاقة الحرة المتحصلة توضح ان الامتزاز الذي يحدث على سطح N80 هو من النوع المختلط كما تشير منحنيات تافل إلى أن البوليمرات المختبرة تعمل كمثبطات أنوديك وكاثودية مختلطة. من ناحية أخرى، وجد أن جميع البوليمرات المحورة أظهرت خصائص متميزة كمضادة للأكسدة وللبيكتيريا.

**الكلمات المفتاحية:** احادي ايثانول امين، اطارات مستهلكة، ثنائي ايثانول امين، ثلاثي ايثانول امين، جهاز الاستقطاب، حامض الفسفوريك، سبيكة N80.